Обзор ArXiv: astro-ph, 24-28 апреля 2017 года

От Сильченко О.К.

Astro-ph: 1704.07839

Lyα ABSORBERS AND THE COMA CLUSTER

Joo Heon Yoon (윤주헌) & M.E. Putman[1]
[1] Department of Astronomy, Columbia University, New York, NY 10027, USA

Abstract

The spatial and kinematic distribution of warm gas in and around the Coma Cluster is presented through observations of Lyα absorbers using background QSOs. Updates to the Lyα absorber distribution found in Yoon et al. (2012) for the Virgo Cluster are also presented. At 0.2-2.0$R_{\rm vir}$ of Coma we identify 14 Lyα absorbers ($N_{\rm HI}$= $10^{12.8-15.9}$ cm^{-2}) towards 5 sightlines and no Lyα absorbers along 3 sightlines within $3\sigma_{\rm v\,coma}$. For both Coma and Virgo, most Lyα absorbers are found outside the virial radius or beyond $1\sigma_{\rm v}$ consistent with them largely representing the infalling intergalactic medium. The few exceptions in the central regions can be associated with galaxies. The Lyα absorbers avoid the hot ICM, consistent with the infalling gas being shock-heated within the cluster. The massive dark matter halos of clusters do not show the increasing column density with decreasing impact parameter relationship found for the smaller mass galaxy halos. In addition, while the covering fraction within $R_{\rm vir}$ is lower for clusters than galaxies, beyond $R_{\rm vir}$ the covering fraction is somewhat higher for clusters. The velocity dispersion of the absorbers compared to the galaxies is higher for Coma, consistent with the absorbers tracing additional turbulent gas motions in the cluster outskirts. The results are overall consistent with cosmological simulations, with the covering fraction being high in the observations standing out as the primary discrepancy.

Virgo & Coma clusters

Table 1. The properties of the Coma and Virgo Clusters

	Coma	Virgo	ref.
$M_{\rm vir}$ ($M_\odot$)	1.4×10^{15}	2.19×10^{14}	a,b
$R_{\rm vir}$ (Mpc)	2.9	1.57	a,b
D (Mpc)	105	16.5	c,d
v (km s^{-1})	6930	1138	e,d
$\sigma_{\rm v}$ (km s^{-1})	1008	544	e,d

NOTE—a: Lokas & Mamon (2003) b: Mamon et al. (2004) c: Ferrarese et al. (2000) d: Mei et al. (2007) e: Struble & Rood (1999)

Coma

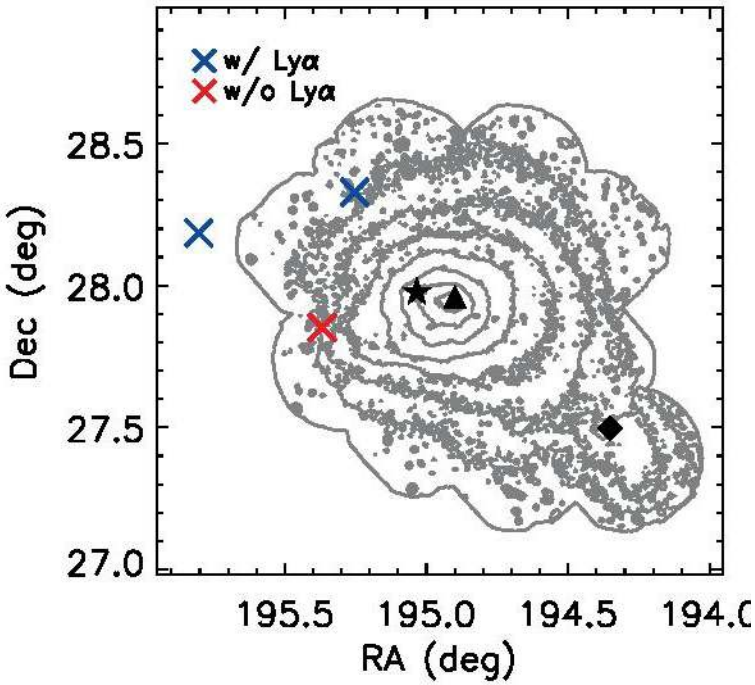

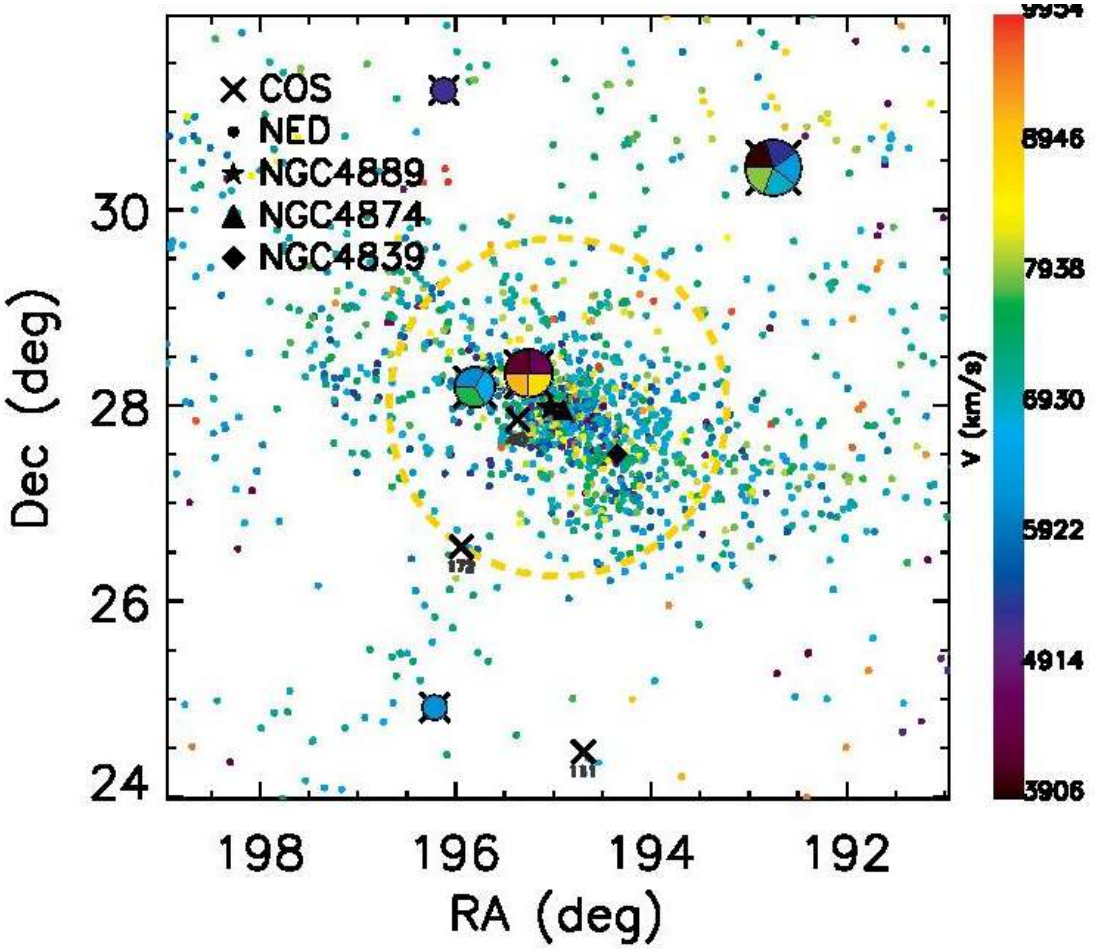

Рентген, центральная часть

Virgo

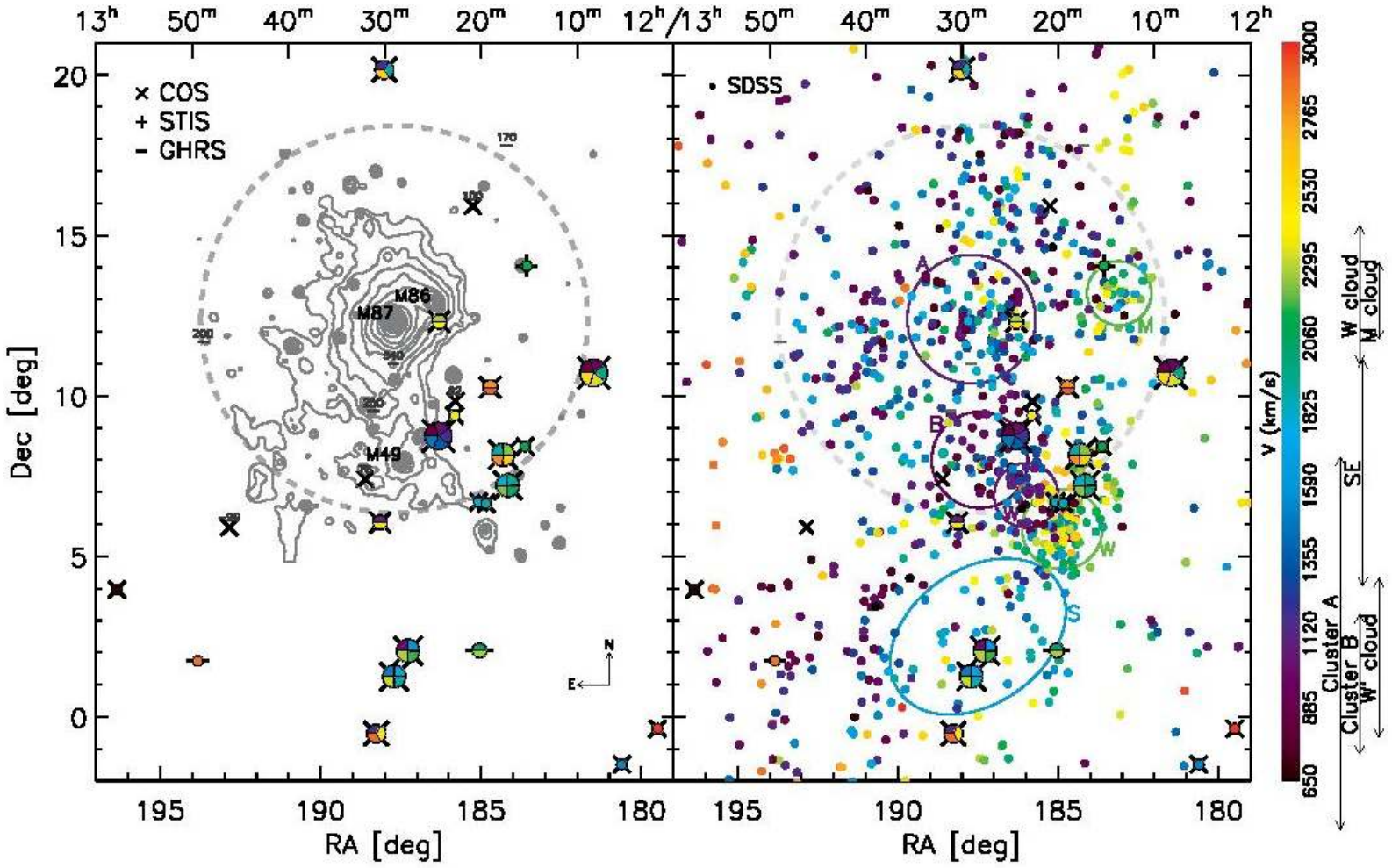
× COS
+ STIS
– GHRS
M86
M87
M49
SDSS
A
B
M
W
S
W cloud
M cloud
SE
Cluster A
Cluster B
W' cloud
v (km/s)
3000
2765
2530
2295
2060
1825
1590
1355
1120
885
650
Dec [deg]
RA [deg]
13h 50m 40m 30m 20m 10m 12h
20
15
10
5
0
195
190
185
180

Все хорошо, но распределение скоростей – не двугорбое…

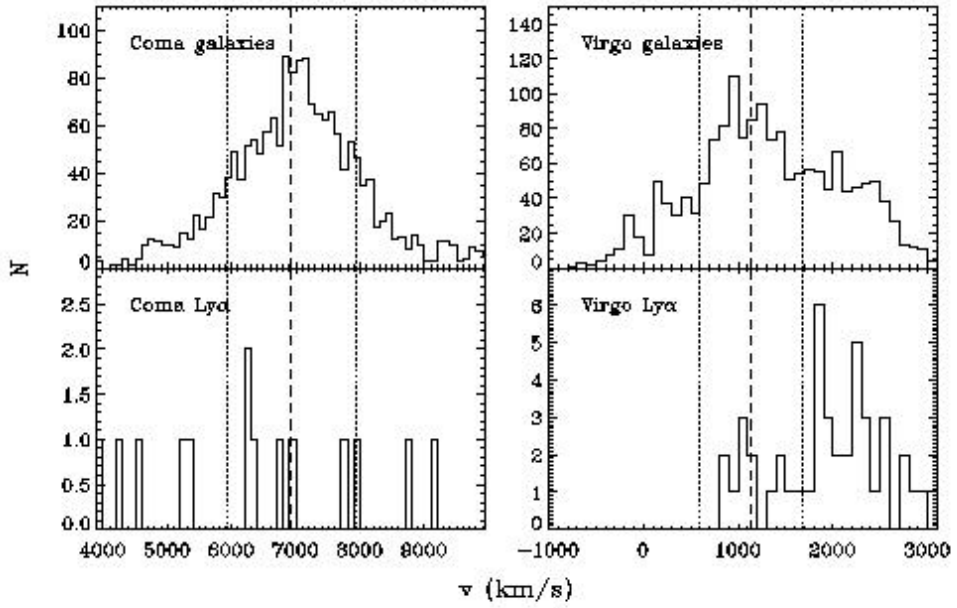

Figure 3. Velocity distribution of galaxies (top) and Lyα absorbers (bottom) for the Coma Cluster (left) and the Virgo Cluster (right). Dashed lines and dotted lines represent the central velocity and velocity dispersion for each cluster.

Astro-ph: 1704.08261

Lessons from the Auriga discs: The hunt for the Milky Way's ex-situ disc is not yet over

Facundo A. Gómez[1⋆], Robert J. J. Grand[2,3], Antonela Monachesi[1], Simon D. M. White[1], Sebastian Bustamante[2], Federico Marinacci[4], Rüdiger Pakmor[2], Christine M. Simpson[2], Volker Springel[2,3], and Carlos S. Frenk[5]

[1] *Max-Planck-Institut für Astrophysik, Karl-Schwarzschild-Str. 1, D-85748, Garching, Germany*
[2] *Heidelberger Institut für Theoretische Studien, Schloss-Wolfsbrunnenweg 35, 69118 Heidelberg, Germany*
[3] *Zentrum für Astronomie der Universitat Heidelberg, Astronomisches Recheninstitut, Monchhofstr. 12-14, 69120 Heidelberg, Germany*
[4] *Department of Physics, Kavli Institute for Astrophysics and Space Research, MIT, Cambridge, MA 02139, USA*
[5] *Institute for Computational Cosmology, Department of Physics, Durham University, South Road, Durham, DH1 3LE, UK*

ABSTRACT

We characterize the contribution from accreted material to the galactic discs of the Auriga Project, a set of high resolution magnetohydrodynamic cosmological simulations of late-type galaxies performed with the moving-mesh code AREPO. Our goal is to

26 моделей Milky Way; у 9ти – больше 5% звезд диска не родные

Run	$M_{\rm vir}$ [10^{10}M$_\odot$]	$R_{\rm vir}$ [kpc]	M_* [10^{10}M$_\odot$]	$M_{\rm d}$ [10^{10}M$_\odot$]	$R_{\rm d}$ [kpc]	$M_{\rm b}$ [10^{10}M$_\odot$]	$R_{\rm eff}$ [kpc]	n	D/T	$R_{\rm opt}$ [kpc]
Au-2	191.466	261.757	7.045	6.377	11.644	2.341	2.056	1.529	0.73	37.0
Au-3	145.777	239.019	7.745	6.288	7.258	2.039	1.488	0.987	0.76	31.0
Au-4	140.885	236.310	7.095	3.662	3.929	2.005	1.740	1.352	0.65	24.5
Au-5	118.553	223.091	6.722	4.509	3.583	1.806	0.839	0.874	0.71	21.0
Au-6	104.385	213.825	4.752	3.315	5.949	1.649	2.851	2.000	0.67	26.0
Au-7	112.043	218.935	4.875	2.458	5.140	2.045	1.731	1.740	0.55	25.0
Au-8	108.062	216.314	2.990	2.457	6.572	0.652	2.147	1.328	0.79	25.0
Au-9	104.971	214.224	6.103	3.597	3.367	2.169	0.999	0.948	0.62	19.0
Au-10	104.710	214.061	5.939	2.378	2.596	3.152	1.080	1.181	0.43	16.0
Au-12	109.275	217.117	6.010	4.315	3.290	1.134	0.892	0.759	0.79	19.0
Au-13	118.904	223.325	6.194	1.675	3.382	3.798	1.403	1.549	0.31	15.5
Au-14	165.721	249.442	10.393	6.359	4.186	3.184	1.138	1.586	0.67	26.0
Au-15	122.247	225.400	3.930	2.772	5.320	1.047	2.216	2.000	0.73	23.0
Au-16	150.332	241.480	5.410	5.059	9.030	1.175	1.825	1.391	0.81	36.0
Au-17	102.835	212.769	7.608	2.563	4.191	4.641	1.208	0.831	0.36	16.0
Au-18	122.074	225.288	8.037	5.205	3.719	2.461	1.225	0.950	0.68	21.0
Au-19	120.897	224.568	5.320	3.532	4.805	1.428	1.416	2.000	0.71	24.0
Au-20	124.922	227.028	4.740	2.248	8.019	2.353	2.174	1.886	0.49	30.0
Au-21	145.090	238.645	7.717	6.005	4.607	1.240	1.188	1.064	0.83	24.0
Au-22	92.621	205.476	6.020	2.851	2.249	2.709	1.014	0.934	0.51	13.5
Au-23	157.539	245.274	9.023	5.547	4.985	3.192	1.708	1.438	0.63	25.0
Au-24	149.178	240.856	6.554	3.756	5.570	2.186	0.946	0.969	0.63	30.0
Au-25	122.109	225.305	3.142	2.475	6.695	0.934	2.951	1.879	0.73	21.0
Au-26	156.384	244.685	10.967	4.697	3.141	5.456	1.116	1.017	0.46	18.0
Au-27	174.545	253.806	9.606	7.229	4.287	1.742	0.947	1.065	0.81	26.0
Au-28	160.538	246.833	10.448	6.761	2.159	2.359	0.948	1.109	0.74	17.5

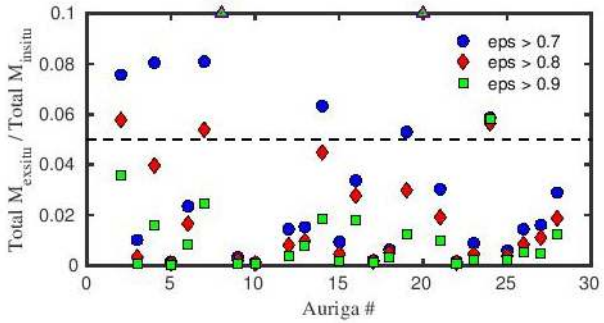

Figure 1. Ratio of the total ex-situ to in-situ disc mass, η, for the different Auriga galaxies. Only stellar particles with $R < R_{\rm opt}$ and $|Z| < 10$ kpc are considered. Blue, red and green symbols indicate the results obtained when a cut in the circularity parameter at 0.7, 0.8 and 0.9 is imposed, respectively. The horizontal dashed lines indicate a 5% mass ratio.

Во внешних частях дисков неродных звезд больше

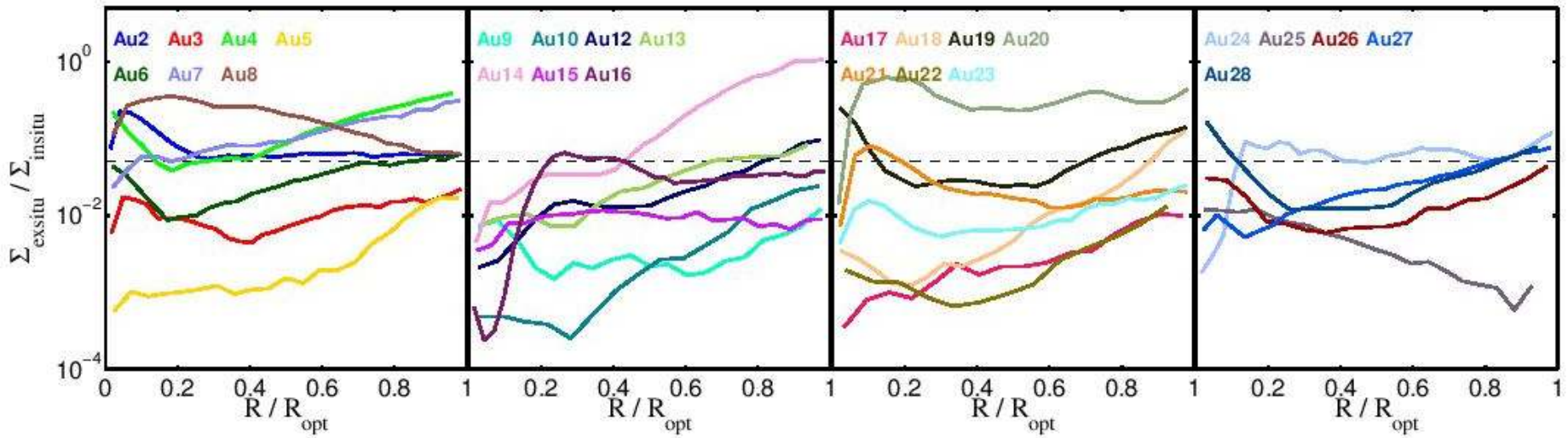

Figure 2. Surface density ratio, $\mu = \Sigma_{\rm exsitu}/\Sigma_{\rm insitu}$, as a function of galactocentric distance for the different Auriga galaxies. For comparison, distances are normalized by the corresponding $R_{\rm opt}$. The horizontal dashed lines indicate a 5% density ratio.

Вид на «неродной» компонент – сверху и сбоку

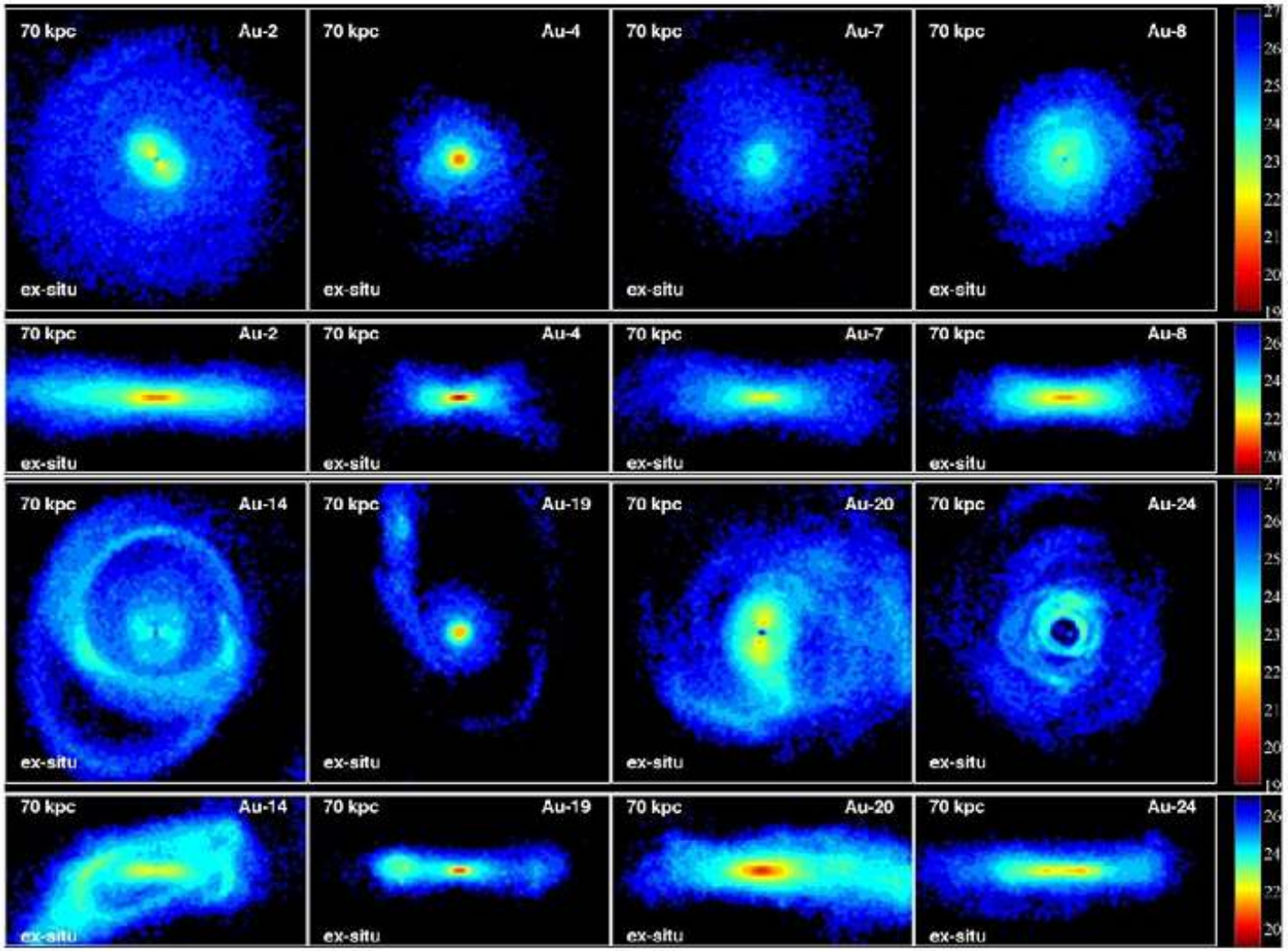

«Родные» звезды – более круговые

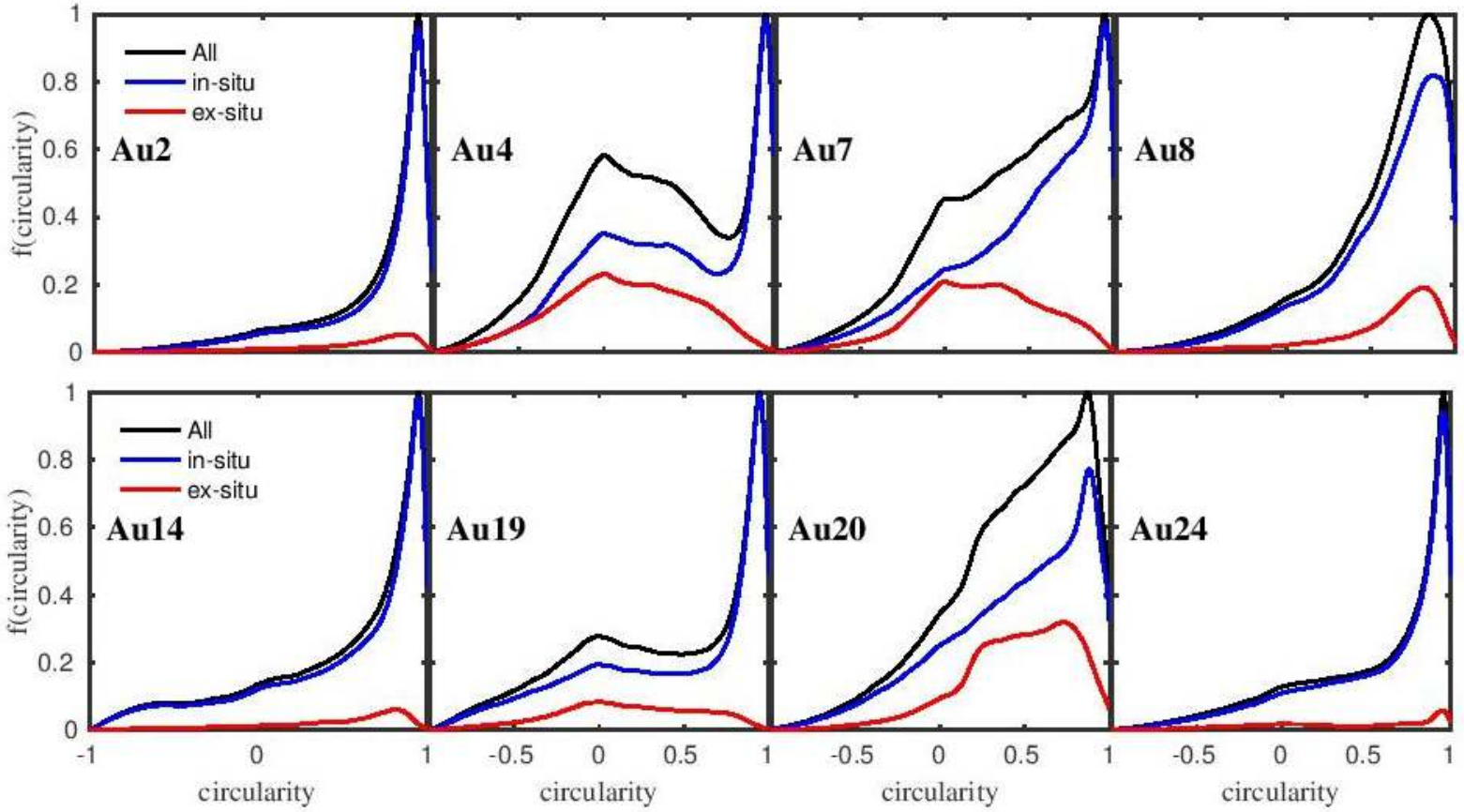

… а также более металличные и с отрицательным градиентом возраста по радиусу.

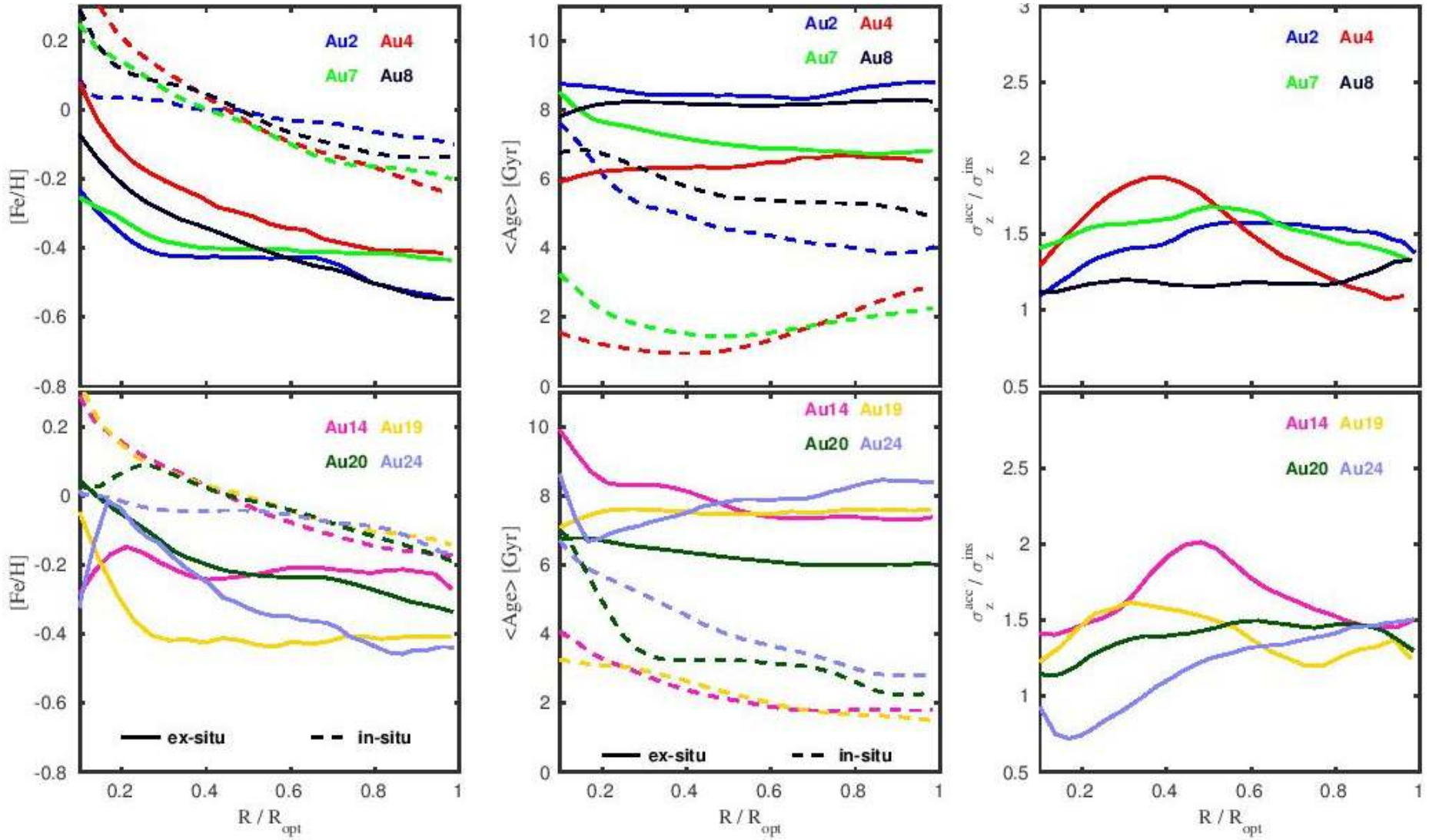

Происхождение: максимум 2 спутника, подстраиваются в плоскость

Table 2. Main properties of the most significant contributors to the ex-situ discs. The columns are 1) Model name, 2) Satellite's peak total mass, 3) Lookback time at which each satellite crosses the host $R_{\rm vir}$ for the first time, and 4) Angle between the angular momentum vectors of the disc and the satellite orbit, measured at $t_{\rm cross}$.

Run	$M_{\rm sat}^{\rm peak}$ $[10^{11}\ M_\odot]$	$t_{\rm cross}$ [Gyr]	$\theta_{\rm infall}$
Au-2	1.2	8.6	45°
	0.9	8.3	45°
Au-4	5.3	3.1	60°
Au-7	1.8	6	85°
Au-8	1.0	8	25°
Au-14	1.0	7.3	45°
	0.8	9.1	30°
Au-19	2.9	5.8	25°
	0.6	7.1	47°
Au-20	2.5	6	15°
Au-24	0.6	8.6	80°

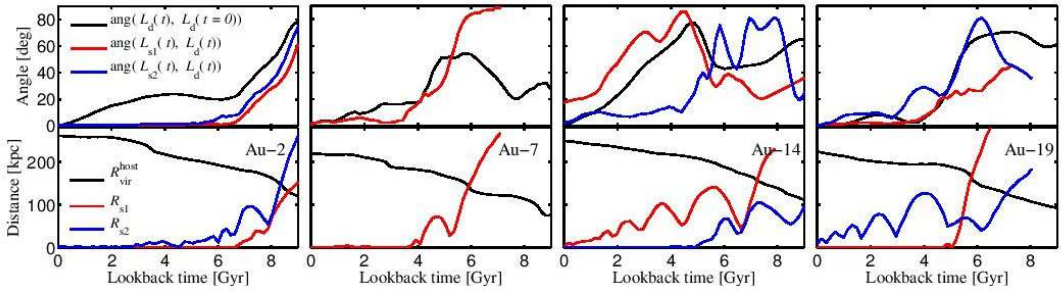

Figure 7. Top panels: The red (blue) lines show the time evolution of the angle between the angular momentum of the disc and that of the orbit of the most significant (second) contributor. The black lines show the time evolution of the orientation of the angular momentum vector of the disc with respect to its orientation at the present-day. Bottom panels: The red (blue) lines show the time evolution of the galactocentric distance of the most significant (second) contributor. The black lines show the time evolution of the host $R_{\rm vir}$.

Astro-ph: 1704.08788

The Multi-Wavelength Tully-Fisher relation with spatially resolved HI kinematics

Anastasia A. Ponomareva[1,2⋆], Marc A. W. Verheijen[2,3] , Reynier F. Peletier[2] and Albert Bosma[4]

[1] *Research School of Astronomy & Astrophysics, Australian National University, Canberra, ACT 2611, Australia*
[2] *Kapteyn Astronomical Institute, University of Groningen, Postbus 800, NL-9700 AV Groningen, The Netherlands*
[3] *Adjunct Faculty, National Centre for Radio Astrophysics, TIFR, Ganeshkhind, Pune 411007, India*
[4] *Aix Marseille Univ, CNRS, LAM, Laboratoire d'Astrophysique de Marseille, Marseille, France*

Выборка

Name	Hubble type	P.A. deg.	Incl. deg.	Distance Mpc
NGC 0055	SB(s)m	110±3	78±7	1.98±0.05
NGC 0224	SA(s)b	37±1	78±1	0.76±0.02
NGC 0247	SAB(s)d	169±3	77±2	3.51±0.09
NGC 0253	SAB(s)c	230±2	77±1	3.56±0.13
NGC 0300	SA(s)d	290±3	46±6	1.97±0.05
NGC 0925	SAB(s)d	283±2	61±5	8.91±0.28
NGC 1365	SB(s)b	218±2	39±8	17.7±0.81
NGC 2366	IB(s)m	42±6	68±5	3.34±0.09
NGC 2403	SAB(s)cd	124±1	61±3	3.17±0.08
NGC 2541	SA(s)cd	170±3	64±4	11.5±0.47
NGC 2841	SA(r)b	150±3	70±2	14.5±0.47
NGC 2976	SAc pec	323±1	61±5	3.63±0.13
NGC 3031	SA(s)ab	330±4	59±5	3.61±0.09
NGC 3109	SB(s)m	92±3	80±4	1.37±0.03
NGC 3198	SB(rs)c	215±5	70±1	13.3±0.55
IC 2574	SAB(s)m	55±5	65±10	3.89±0.14
NGC 3319	SB(rs)cd	33±2	57±4	13.0±0.53
NGC 3351	SB(r)b	192±1	47±5	10.4±0.28
NGC 3370	SA(s)c	327±3	55±5	26.1±0.72
NGC 3621	SA(s)d	344±4	65±7	6.72±0.18
NGC 3627	SAB(s)b	172±1	58±5	9.03±0.29
NGC 4244	SA(s)cd	222±1	88±3	4.61±0.19
NGC 4258	SAB(s)bc	331±1	72±3	7.31±0.16
NGC 4414	SA(rs)c?	160±2	52±4	17.8±0.74
NGC 4535	SAB(s)c	180±1	41±5	16.1±0.66
NGC 4536	SAB(rs)bc	300±3	69±4	14.6±0.60
NGC 4605	SB(s)c pec	293±2	69±5	5.54±0.25
NGC 4639	SAB(rs)bc	311±1	42±2	22.0±0.71
NGC 4725	SAB(r)ab pec	30±3	50±5	12.5±0.46
NGC 5584	SAB(rs)cd	152±4	44±4	22.4±0.72
NGC 7331	SA(s)b	169±3	75±3	13.8±0.51
NGC 7793	SA(s)d	290±2	50±3	3.58±0.11

Table 1. The Tully-Fisher Calibrator Sample. Column (1)

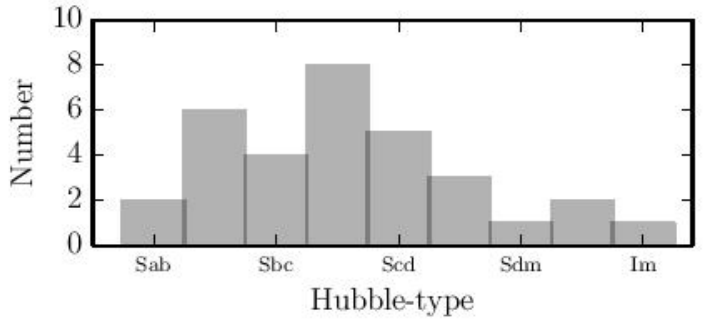

Figure 1. The distribution of morphological types of the galaxies in our sample.

Фотометрия в 12ти полосах

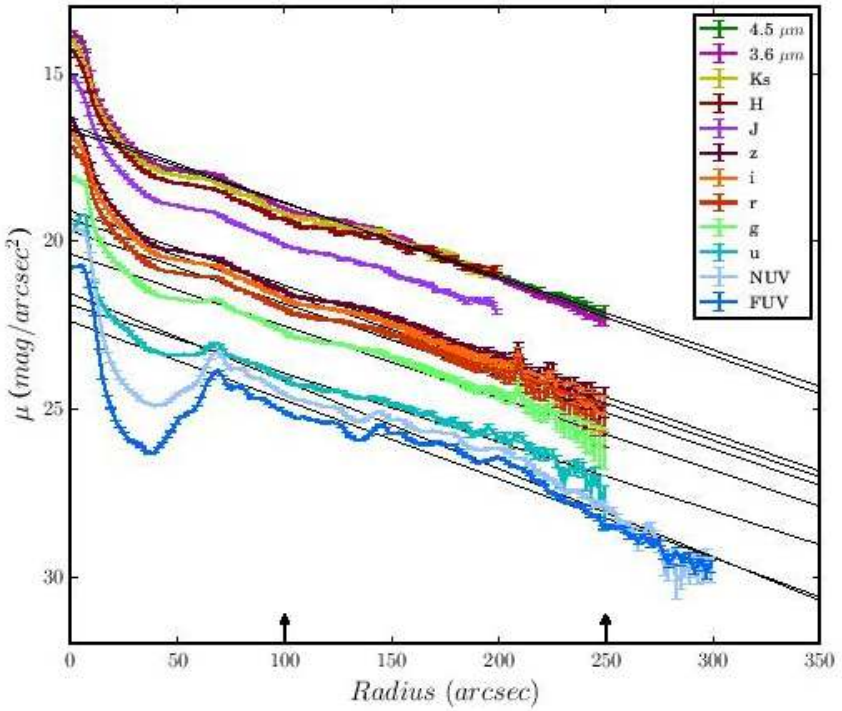

Figure 2. Surface brightness profiles of NGC 3351 for 12 photometric bands. The region within which the exponential disk fit was done is indicated with arrows. Black lines show the exponential disk fit to the profile. Profiles are terminated at their R_{lim}.

Кривые вращения – по интерферометрии в линии 21см

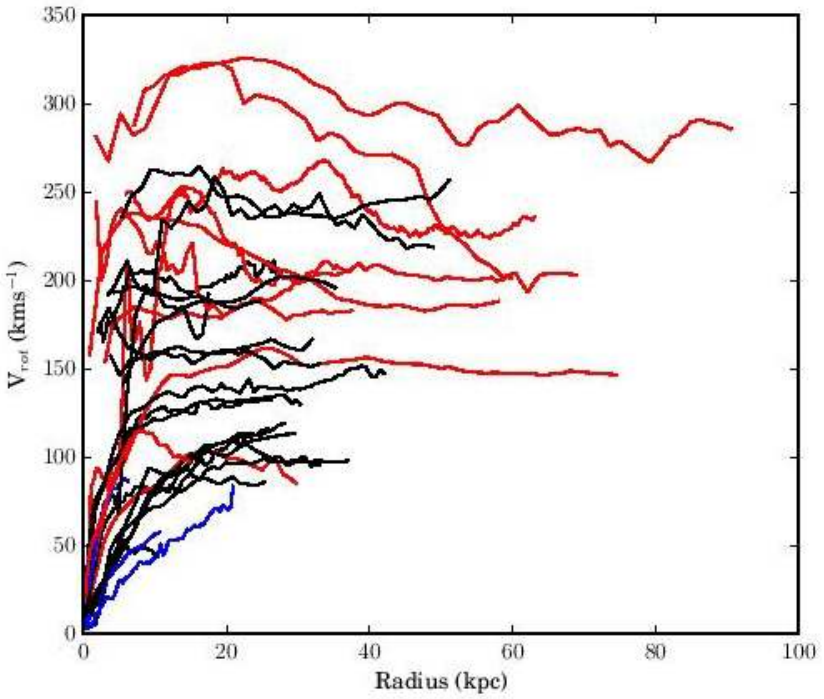

Figure 3. Compilation of extended HI rotation curves of our sample galaxies plotted on the same linear scale. Blue curves belong to galaxies with Rrc ($V_{max} < V_{flat}$) and red curves are declining rotation curves ($V_{max} > V_{flat}$).

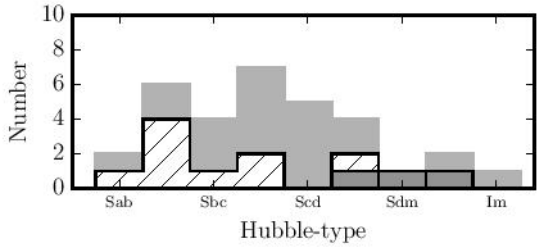

Figure 4. Rotation curves morphology distribution within the sample. The light hatched region shows galaxies with declining rotation curves. The dark shaded area corresponds to galaxies with rising rotation curves.

Форма кривых вращения

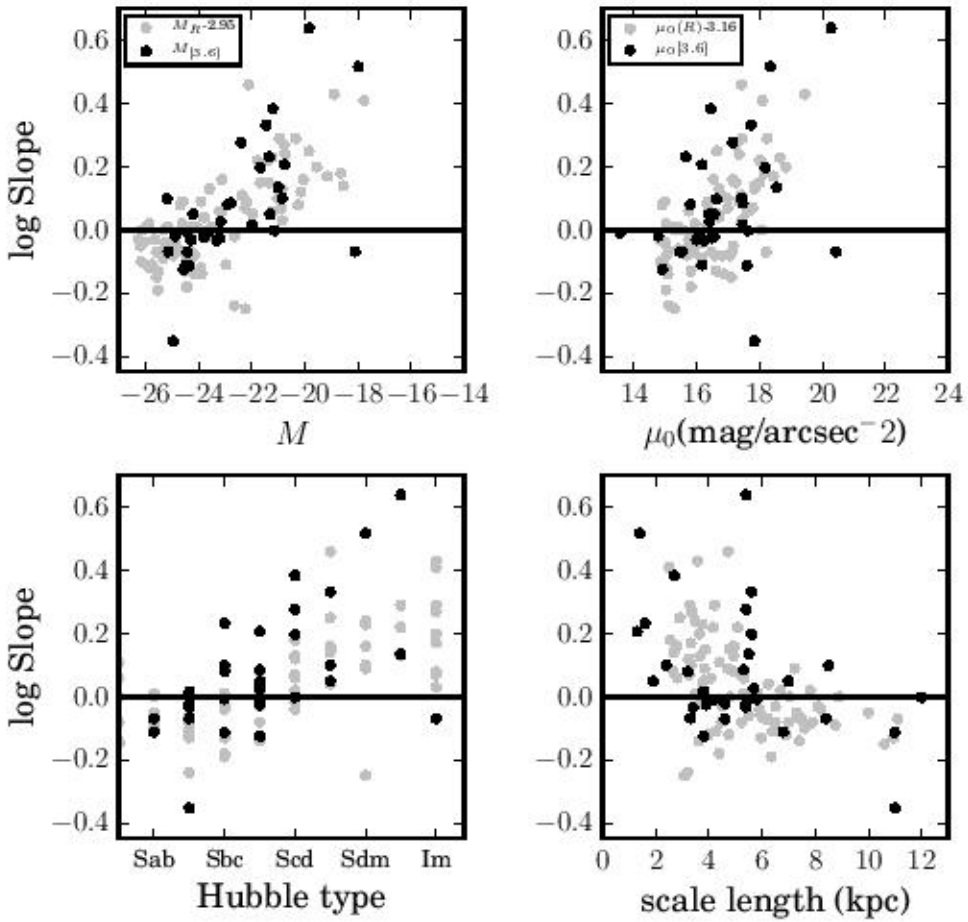

$$S_{2.2h,lmp} = \frac{Log(V_{2.2h}/V_{lmp})}{Log(R_{2.2h}/R_{lmp})} \qquad (3)$$

Вертикальный разброс – это еще не все…

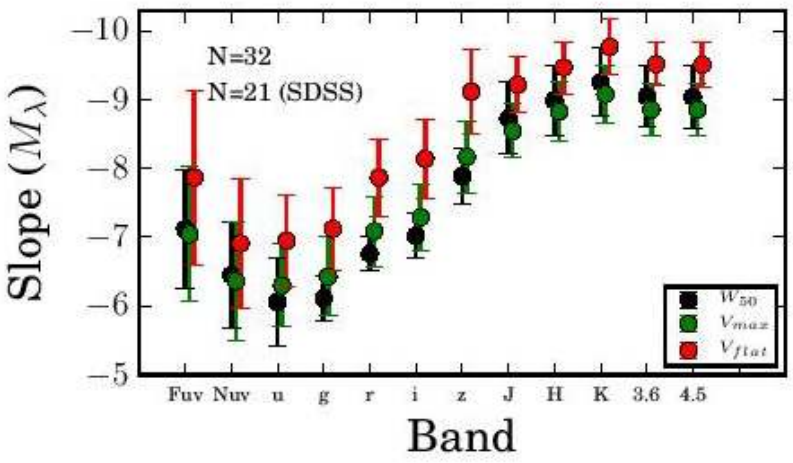

Figure 7. Slope of the TFr as a function of wavelength, calculated using different rotation measures. With black points indicated slopes measured for the TFr based on W^i_{50}, with green based on V_{max} and with red based on V_{flat}. Independently of band, the Tfr based on V_{flat} demonstrates the steepest slope.

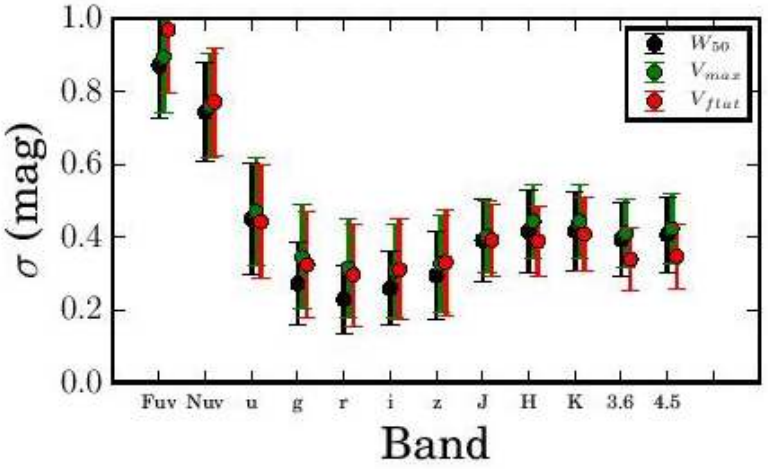

Figure 8. The vertical scatter of the TFr as a function of wavelength, calculated using different rotation measures. With black points indicating the scatter measured for the TFr based on W^i_{50}, with green based on V_{max} and with red based on V_{flat}.

Важнее – перпендикулярный разброс!

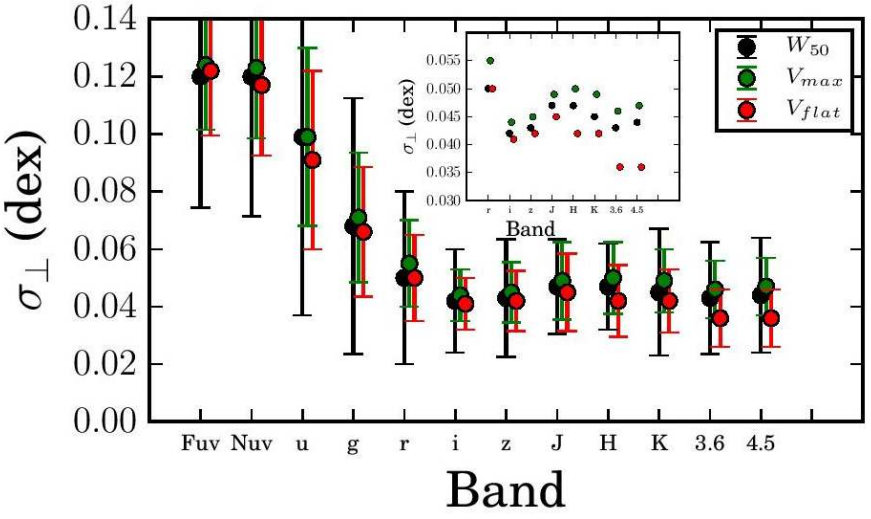

Band	$\sigma_\perp$ (dex)		
	W_{50}^i	V_{max}	V_{flat}
FUV	0.12±0.045	0.124±0.022	0.122±0.022
NUV	0.12±0.048	0.123±0.024	0.117±0.024
u	0.099±0.062	0.099±0.031	0.091±0.031
g	0.068±0.044	0.071±0.022	0.066±0.022
r	0.05±0.03	0.055±0.015	0.05±0.015
i	0.042±0.018	0.044±0.009	0.041±0.009
z	0.043±0.02	0.045±0.01	0.042±0.01
J	0.047±0.016	0.049±0.013	0.045±0.013
H	0.047±0.015	0.050±0.012	0.042±0.012
K	0.046±0.022	0.049±0.011	0.042±0.011
3.6	0.043±0.019	0.046±0.01	0.036±0.01
4.5	0.044±0.02	0.047±0.01	0.036±0.01

Table 5. Tightness of the TFrs in different photometric bands measured in dex. Column (1): photometric band; Column (2)-Column(4): tightness of the TFrs based on W_{50}^i, V_{max} and V_{flat}, measured in dex;

Рекомендуемый вариант – фотометрия 4 мкм и скорость вращения на плоском участке кривой

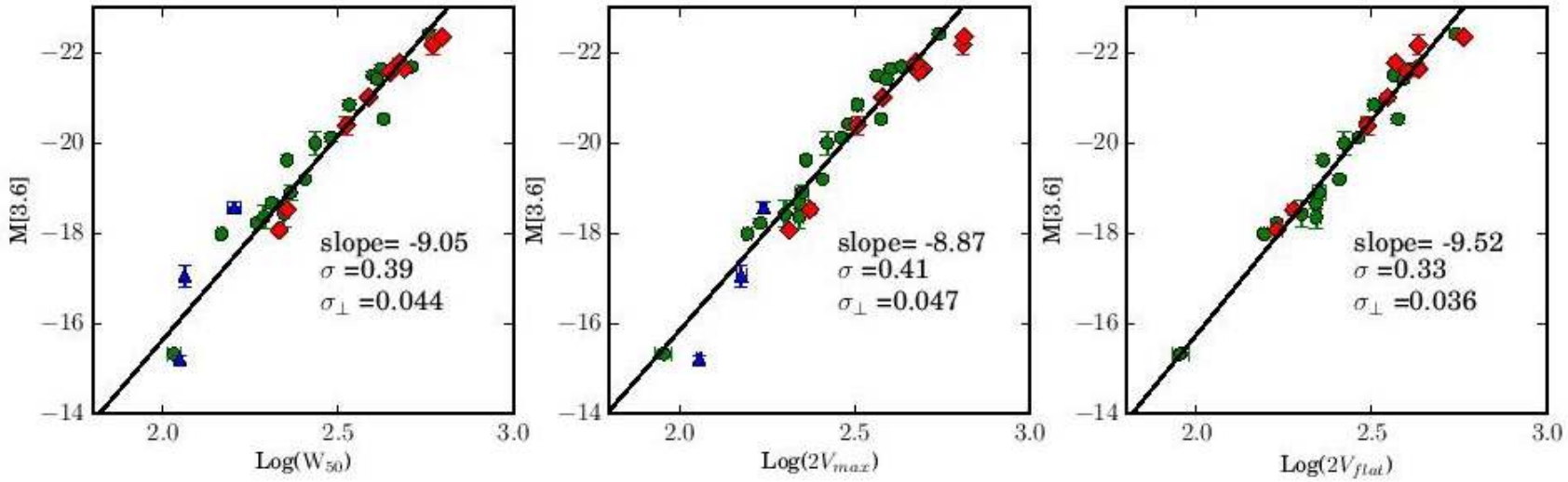

Figure 10. The 3.6 μm TFrs based on the different kinematic measures W_{50}^{i} – left, V_{max} – middle and V_{flat} – right. Green symbols show flat rotation curves ($V_{max} = V_{flat}$), and red symbols indicate galaxies with declining rotation curves ($V_{max} > V_{flat}$). Blue symbols indicate galaxies with rising rotation curves ($V_{max} < V_{flat}$). These galaxies were not included when fitting the model.